Compound fault diagnosis of rolling bearings based on improved tunable Q-factor wavelet transform

OPEN ACCESS
IOP Publishing
Measurement Science and Technology
Meas. Sci. Technol. **32** (2021) 105018 (15pp)
https://doi.org/10.1088/1361-6501/abf25e

Compound fault diagnosis of rolling bearings based on improved tunable Q-factor wavelet transform

Yongtao Hu[1,2,*], Qiang Zhou[2], Jinfeng Gao[3], Jie Li[1] and Yonggang Xu[4]

[1] School of Electrical Engineering and Automation, Henan Institute of Technology, Xinxiang 453000, People's Republic of China
[2] Intelligent Research Institute, Henan Weihua Heavy Machinery Co., Ltd, Changyuan 453400, People's Republic of China
[3] School of Electrical Engineering, Zhengzhou University, Zhengzhou 450000, People's Republic of China
[4] College of Mechanical Engineering and Applied Electronics Technology, Beijing University of Technology, Beijing 100124, People's Republic of China

E-mail: hythait@163.com

Received 23 December 2020, revised 21 March 2021
Accepted for publication 26 March 2021
Published 5 July 2021

Abstract

In order to solve the difficulty of compound fault diagnosis of rolling bearings, a novel rolling bearings fault diagnosis method based on improved tunable Q-factor wavelet transform (TQWT) is proposed in this paper. Firstly, a new evaluation index of signal decomposition called KR is defined by summing kurtosis and root mean square (RMS) with weight. KR is the compromise between impulse factor and energy factor, which can better represent the fault characteristics of sub-bands obtained by TQWT. Secondly, the KR is used to improve the TQWT. The improved TQWT can adaptively determine the parameters Q-factor and decomposition level. Thirdly, the bearing vibration signal is decomposed by the improved TQWT and the sub-bands are sorted descending according to the KR. Finally, the Hilbert envelope analysis is carried out and the fault types are determined by comparing the fault characteristic frequencies obtained from the Hilbert envelopes to the fault characteristic frequencies calculated by formula. The proposed fault diagnosis method is fully evaluated by simulation and experiments. The results demonstrate that the KR takes advantage of kurtosis and RMS and can be better used to optimize the parameter of TQWT. And the compound fault features of rolling bearings can be accurately separated into different sub-bands by the improved TQWT, which is helpful to improve the accuracy of compound fault diagnosis of rolling bearings.

Keywords: rolling bearings, compound fault diagnosis, improved TQWT, evaluation index, Hilbert envelope

(Some figures may appear in colour only in the online journal)

* Author to whom any correspondence should be addressed.

1. Introduction

Rolling bearings are essential components of rotating machinery. Due to long term running in complicated conditions such as variable speeds, alternating and heavy loads, bearings are damaged inevitably. Abundant engineering practice shows that compound faults are more frequent in rolling bearings, such as the inner ring race and outer race of a bearing are worn to different degrees at the same time, which makes the bearing vibration signals complex, nonlinear and nonstationary [1]. Together with that, the weak fault features are often submerged by the strong fault features, resulting in inaccurate fault diagnosis. So, compound fault diagnosis of bearings becomes an urgent problem to be solved. An effective method of compound fault diagnosis of bearing is extremely valuable to ensure the safe and stable operation of the mechanical equipment [2].

Currently, many vibration signal processing methods have been developed to extract the fault features and realize the diagnosis of compound fault that appears on the bearings [3–5]. Wavelet transform is the most used method [6–8]. Purushotham *et al* [9] used the discrete wavelet transform (DWT) to extract the bearing compound fault features and applied hidden Markov models to detect single and compound fault in bearing. Dhamande *et al* [10] extracted compound fault features by conducting both continuous and DWT to the vibration signals. Chen *et al* [11] proposed an improved adaptive redundant lifting multi-wavelet method to extract all the features of compound faults. The above methods are based on the traditional wavelet transform, whose effectiveness is affected by the Q-factor. Q-factor denotes the central frequency of the wavelet. Generally, the wavelet transform should have a high Q-factor when it is used for processing the signal with more oscillatory behavior. On the other hand, it should have a low Q-factor when the signal has little oscillatory behavior. Namely, the Q-factor must be chosen according to the oscillatory behavior of the signal, but it is difficult and time consuming for the traditional wavelet transform, because it not only depends on the signal, but also the wavelet base function [12]. For the problem of above, the tunable Q-factor wavelet transform (TQWT) was proposed by Selesnick [13]. TQWT is a new flexible fully-DWT. It can decompose the vibration signal into sustained oscillation component (high Q-factor) and transient impact component (low Q-factor) through variable Q-factor [14]. The main advantage of TQWT is that there is no need to care about the selection problems of the wavelet base function, and the Q-factor can be ajusted flexibly according to the signal. This make TQWT easier and more effective for vibration signal processing and suitable for fault feature extraction [15, 16].

Although, the Q-factor of TQWT can be flexibly adjusted, this does not mean that it can be selected randomly. In fact, the selections of Q-factors and decomposition level of TQWT heavily affect the decomposition performance. The main challenge becomes the optimizations of Q-factors and decomposition level when TQWT is used for fault diagnosis. Nowadays, many reasearchers have focused on the optimization of Q-factors, of which kurtosis-based method is the mostly used method to improve the TQWT [17]. Kurtosis is an effective index to characterize the impulsive feature. The kurtosis of the vibration signal will be greater when the bearing occurs fault. It is the most used index to select the parameters of a decomposition method [18–20]. Parameters of TQWT can be selected according to the kurtosis maximum principle [21]. Li *et al* [22] proposed an incipient fault diagnosis method of bearing based on maximal spectral kurtosis TQWT and group sparsity total variation denoising. In this method the Q-factor of TQWT is pre-selected according to spectral distribution of the impulse component and then the spectral kurtosis of each scale transform coefficients is calculated to select the optimal Q-factor according to the kurtosis maximum principle. Wang *et al* [23] proposed an adaptive tunable Q-factor wavelet transform based on time-frequency kurtosis index optimization to realize the early fault diagnosis of bearings. They used kurtosis to search the Q-factor and the redundancy. Ma *et al* [24] proposed a early fault diagnosis of bearing based on frequency band extraction and improved TQWT. Particle swarm optimization (PSO) was used to improve the TQWT and the kurtosis was taken as the fitness of PSO to determine the Q-factor.

Although kurtosis can be used to optimize the Q-factor, kurtosis is very sensitive to the discrete outliers in the sub-bands obtained by the TQWT. The outliers make the kurtosis fail, it means that some sub-band has a big kurtosis, but the sub-band does not contain fault features. So, kurtosis cannot better evaluate the sub-bands obtained by the TQWT. Especially when the bearing has a compound fault. In order to solve this problem, an improved evaluation index is extremely necessary. Root mean square (RMS) reflects the energy factor of the vibration signal [25]. It is gentler than kurtosis and insensitive to the discrete outliers in sub-bands. RMS increases when a bearing works in the fault conditions. But the weak fault feature may be neglected due to the interference of noise in some sub-bands. Taking advantages of kurtosis and RMS and overcoming its weakness, a new evaluation index can be defined, which can be used as the index to improve the TQWT and optimizing the Q-factor. On the other hand, there are little reasearches consider the optimization of the decomposition level. A lot of sub-bands will be obtained when the vibrational signal is decomposed by TQWT with the the max decomposition level. This will result the difficult of which sub-band to be selected for further analyzing. So, the decomposition level should be optimized meanwhile.

In order to sovle the above problem, a new evaluation index called KR was defined based on kurtosis and RMS in this paper. Then, KR is used to improve the TQWT by simultaneously optimizing the Q-factor and the decomposition level. Finally, a new method based on the improved TQWT was proposed to solve the difficulty of compound fault diagnosis of rolling bearings. The effective of the proposed method is fully evaluated by simulation and experiment.

The rest of the paper is organized as follows. In section 2, the improved TQWT is detailed. Section 3 proposes the compound fault diagnosis method of rolling bearings based on the improved TQWT. In section 4, simulation and experiment are performed to validate the effectiveness of the method.

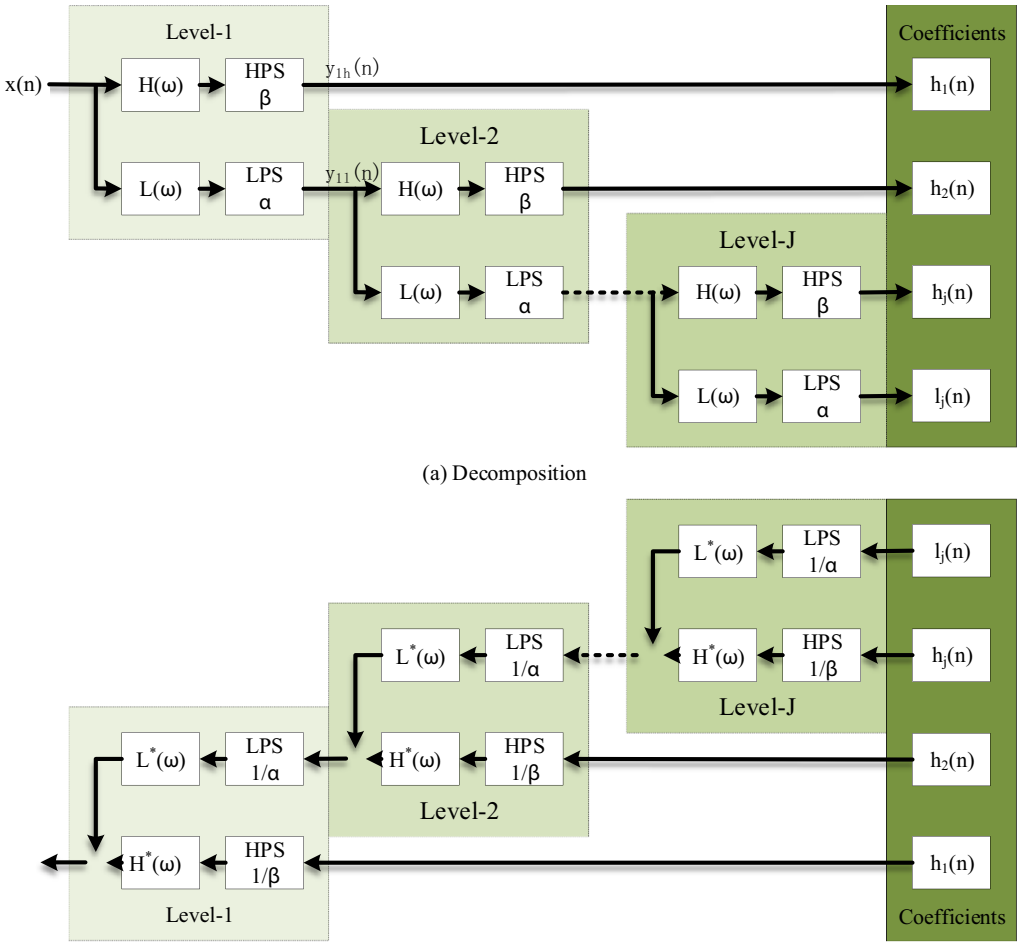

Figure 1. Decomposition and reconstruction of signal x by J-levels TQWT.

Finally, the conclusions are drawn in section 5 and some future directions are suggested.

2. Improved TQWT

2.1. TQWT

TQWT has properties of fully discrete, perfect reconstruction, modestly overcomplete and easy to implement. It is achieved by iteratively applying high pass filter bank followed by high pass scaling (HPS β) and low pass filter followed by low pass scaling (LPS α) on its low pass channel. Decomposition and reconstruction of the signal $x(n)$ by J-levels TQWT is illustrated in figure 1.

The sub-band signals after level-1 processing of high pass and low pass have sampling rates of βf_s and αf_s respectively, where f_s is the sampling rate of the input signal $x(n)$. The scaling parameters α and β satisfy:

$$0 < \alpha < 1\ ,\ 0\langle\beta \leqslant 1\ ,\ \alpha+\beta\rangle 1. \tag{1}$$

In order to perfect reconstruction, the frequency responses of high pass filter $H(\omega)$ and low pass filter $L(\omega)$ are defined respectively as follows:

$$H(\omega) = \begin{cases} 0, & |\omega| \leqslant (1-\beta)\pi \\ \theta\left(\dfrac{\alpha\pi-\omega}{\alpha+\beta-1}\right), & (1-\beta)\pi < |\omega| < \alpha\pi \\ 1, & \alpha\pi \leqslant |\omega| \leqslant \pi \end{cases} \tag{2}$$

$$L(\omega) = \begin{cases} 1, & |\omega| \leqslant (1-\beta)\pi \\ \theta\left(\frac{\omega+(\beta-1)\pi}{\alpha+\beta-1}\right), & (1-\beta)\pi < |\omega| < \alpha\pi \\ 0, & \alpha\pi \leqslant |\omega| \leqslant \pi \end{cases} \tag{3}$$

where $\theta(\omega)$ is the Daubechies frequency response with two vanishing moments [26].

$$\theta(\omega) = \frac{(1+\cos\omega)\sqrt{2-\cos\omega}}{2},\ |\omega| \leqslant \pi. \tag{4}$$

It can be proven that $|H(\omega)|^2 + |L(\omega)|^2 = 1$. So, the high pass filter and the low pass filter satisfy the perfect reconstruction requirement.

Analyzing the iteration of J-levels filters and scalings, the equivalent high pass filter and low pass filter can be expressed as follows.

$$H^{(j)}(\omega)=\begin{cases}H(\omega/\alpha^{j-1})\prod_{n=0}^{j-2}L(\omega/\alpha^{n}),\ \omega_1\leqslant|\omega|\leqslant\omega_2\\ 0,\ \text{for other}\ \omega\in[-\pi,\pi]\end{cases}\tag{5}$$

$$L^{(j)}(\omega)=\begin{cases}\prod_{n=0}^{j-1}L(\omega/\alpha^{n}),\ |\omega|\leqslant\alpha^{j}\pi\\ 0,\ \alpha^{j}\pi\leqslant|\omega|\leqslant\pi\end{cases}\tag{6}$$

where $\omega_1=(1-\beta)\alpha^{j-1}\pi$, $\omega_2=\alpha^{j-1}\pi$. According to the above analysis, the property of TQWT is related to three parameters, namely the decomposition level, the scaling parameters α and β. Q-factor is defined as the ratio of the center frequency ω_c to the bandwidth BW of the filter.

$$Q=\frac{\omega_c}{\mathrm{BW}}.\tag{7}$$

According to equation (7), the band width BW can be approximated as follows:

$$\mathrm{BW}=\frac{\omega_2-\omega_1}{2}=\frac{\beta\alpha^{j-1}\pi}{2}.\tag{8}$$

And the center frequency can be approximately taken as the average of ω_1 and ω_2.

$$\omega_c=\frac{\omega_1+\omega_2}{2}=\frac{(2-\beta)\alpha^{j-1}\pi}{2}.\tag{9}$$

Then, the Q-factor can be calculated.

$$Q=\frac{2-\beta}{\beta}.\tag{10}$$

Equation (10) shows that Q-factor depends only on the HPS β, does not depend on the level J and the LPS α.

The total over-sampling rate of the TQWT is defined as the redundancy of the wavelet transform as follows:

$$r=\frac{\beta}{1-\alpha}.\tag{11}$$

The relationship between the high-pass scaling parameter β, low-pass scaling parameter α, Q and r can be summarized as follows:

$$\beta=2/(Q+1)\tag{12}$$

$$\alpha=1-\beta/r.\tag{13}$$

It is obvious that the performance of TQWT is affected by three parameters: the Q-factor (Q), the redundancy (r) and the decomposition level (J). Q affects the oscillations behaviors of the wavelet. The higher is the Q, the more oscillatory cycles comprising a pulse. When r is close to 1.0, the wavelet will not be well localized in time domain, so a value of 3.0 or greater is recommended [27]. J is the number of filter banks. It determines the decomposition level. The maximum number of allowable decompositions ($J_{\max}$) can be calculated using Q and r.

$$J_{\max}=\left\lfloor\log\left(\frac{N}{4(Q+1)}\right)\Big/\log\left(\frac{Q+1}{Q+1-r/2}\right)\right\rfloor\tag{14}$$

where N is the data length and symbol $\lfloor\bullet\rfloor$ represents round down.

2.2. Evaluation index KR

According to above discussion, it is quite important to determine the parameters of TQWT for the feature separation. The first difficulty is the determination of parameter Q. The sub-bands would not contain enough impact characteristics if Q is too big. If Q is too small, there will be frequency aliasing among the sub-bands. Fortunately, the characteristics and quality of sub-bands can be evaluated by some performance indexes, such as kurtosis and RMS.

Kurtosis is sensitive to the impulse vibration caused by bearing failure and widely used in fault diagnosis. The kurtosis of a signal x is defined as follows:

$$K=E\{(x-\mu)^4\}\Big/\sigma^4\tag{15}$$

where $E\{\bullet\}$ denotes the expectation, μ and σ are the mean and standard deviation of x, respectively. The bigger the sub-band kurtosis is, the more obvious the fault features are. So, several sub-bands with bigger kurtosis can be selected for further analysis to realize fault diagnosis according to the kurtosis maximum principle. Noted that there would be discrete outliers in some sub-bands obtained by TQWT. The discrete outliers will lead to the sharp increase of kurtosis, but the sub-bands do not contain fault information. In order to solve this problem, anther index is need to be involved.

The RMS of the signal x is defined as follows:

$$R=\sqrt{\frac{1}{N}\sum_{i=1}^{N}x_i^2}\tag{16}$$

where N is the length of x. The RMS reflects the average energy of the vibration signal. It is gentler than kurtosis and insensitive to the discrete outliers in sub-bands. When the failure of bearing emerges, the impulse vibration increases the RMS. The bigger RMS means the more fault features in most sub-bands. However, the weak fault feature may be neglected by the noise in some sub-bands. Namely, maybe the RMS of the sub-band is big, but it does not contain obvious fault features or the fault feature cannot be extracted.

To overcome the weakness and take advantage of kurtosis and RMS, a new evaluation index can be defined. The problem is transformed into the fusion of kurtosis and RMS. According to above researches, sub-bands with bigger kurtosis or RMS can be selected for further analysis. However, experiments have showed that there are some sub-bands with bigger kurtosis or RMS, but the sub-bands do not contain clear fault features. Due to the weakness of kurtosis and RMS, these sub-bands usually have bigger kurtosis but smaller RMS or have bigger RMS but smaller kurtosis. This problem can be solved by sum the kurtosis and RMS with weights.

The sequence of kurtosis and RMS of all sub-bands can be expressed as $[K_1, K_2, \cdots, K_J]$ and $[R_1, R_2, \cdots, R_J]$ respectively. The standard deviation of a sequence reflects the fluctuation of the sequence. The smaller the standard deviation is, the more reliable and stable the sequence is, the more effective information the sub-band can provide. So, the indexes sequence with smaller standard deviation should have a bigger weight. On the other hand, the indexes sequence with bigger standard deviation should have a smaller weight. Take σ_R and σ_K as the standard deviation of the sequence of kurtosis and RMS, respectively. The kurtosis weight w_K and RMS weight w_R can be respectively calculated as follows:

$$w_K = \sigma_R / (\sigma_K + \sigma_R) \tag{17}$$

$$w_R = \sigma_K / (\sigma_K + \sigma_R). \tag{18}$$

It is obvious that the w_K is bigger than w_R when σ_K is smaller than σ_R. The new evaluation index could be defined as KR:

$$KR(i) = w_K K_i + w_R R_i, \quad i = 1, 2, \cdots J. \tag{19}$$

In fact, the KR is the compromise between impulse factor and energy factor. It can ensure that the sub-band with bigger kurtosis has bigger RMS. Only the sub-bands have both bigger kurtosis and bigger RMS contain the clear fault features. So, the KR can be used as the evaluation index of sub-bands. The larger the KR is, the more obvious fault features the sub-bands have. So, the next is to improve the TQWT by KR.

2.3. Improved TQWT based on KR

As discussed above, the property of TQWT decomposition is affected by three parameters: the redundancy (r), the Q-factor (Q) and the decomposition level (J). The improvement of TQWT is mainly focus on these parameters.

The parameter r is the redundancy of TQWT when it is computed using infinitely many levels. It can be interpreted as a measure of how much spectral overlap exists between adjacent band-pass filters. In practical application, it is suggested to set $r \geqslant 3$ [28]. The influence of different parameters on the decomposition performance can be qualitatively observed by normalized frequency response of TQWT. The frequency responses for different r with a fixed Q and J ($Q = 3$ and $J = 8$ for example) is shown in figure 2.

It shows that the parameter r localizes the wavelet in the time domain without changing its shape. For a fixed Q and J, the overlap of the adjacent frequency responses increases with increased value of the parameter r. It results in the failure of covering the entire frequency region when r is too big. To cover the entire frequency region, J should be increased correspondingly, which will increase computational complexity. Considering the computation efficiency, we set $r = 3$ in this paper.

According to the equation (14), for a given signal $x(t)$ with length N, the max decomposition level $J_{\max}$ only relies on the Q when the parameter r is determined. However, if the decomposition level is set to $J_{\max}$, there will be $J_{\max} + 1$ sub-bands. It means that many sub-bands will be obtained, but not all sub-bands contain fault features, which leads to another selection problem of sub-bands. Take $N = 8192$, $Q = 3$ and $r = 3$ for example, 13 sub-bands will be obtained. It can be proved that not all sub-bands contain fault features and only a few sub-bands contain the fault features. It means that there are lots of invalid redundant sub-bands. It is advisable to take some sub-bands for further analysis to realize fault diagnosis, not take all sub-bands for analysis. But the selection of sub-bands for further analysis will not only increase the computational complexity, but also reduce the accuracy of fault diagnosis. In order to decrease the computational complexity and increase the accuracy of fault diagnosis, the decomposition level J should be reduced appropriately.

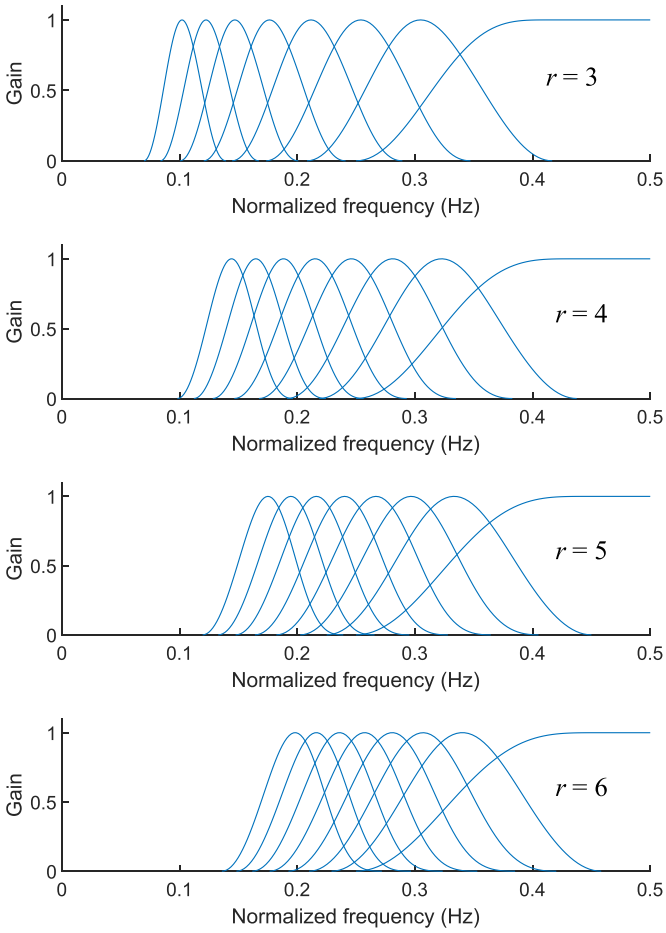

Figure 2. Frequency responses of TQWT for different r with $Q = 3$ and $J = 8$.

In this paper, J is set according to the frequency response bandwidth limitation criteria. Suppose the sample rate of a signal is f_s, then the frequency response bandwidth of the jth sub-band can be determined as follows:

$$B_j = \frac{1}{2}\beta\alpha^{j-1} f_s. \tag{20}$$

It is obvious that the bigger the level is, the smaller the bandwidth is. It is stipulated that the bandwidth of the

Table 1. Calculation method of fault characteristic frequency of bearings.

Fault type	Calculation formula
Inner race fault	BPFI $= n \times$ BPI
Outer race fault	BPFO $= n \times$ BPO
Rolling elements fault	BSF $= n \times$ BS
Cage fault	FTF $= n \times$ FT

sub-band with the maximum level should not be less than three times the maximum fault characteristic frequency $f_{\max}$, namely:

$$\frac{1}{2}\beta\alpha^{j-1}f_s \geqslant 3f_{\max}. \tag{21}$$

The decomposition level J is determined by substituting the equations (20) and (21) into the equation (14) as follows:

$$J = \lfloor 1 + \log(a)/\log(b) \rfloor \tag{22}$$

where $a = 6(Q+1)f_{\max}/f_s$ and $b = 1 - 2/(Q+1)r$. The decomposition level J is decreased and related to the Q. It should mention that the number of sub-bands is small, there is no need to select which sub-band should be taken for further analysis. In fact, all sub-bands should be analyzed.

So, the next is to determine the Q, and the decomposition level J can be determined simultaneously according to the equation (22). As a result, the basic idea of the improved TQWT is automatically determine the optimal parameters Q and J according to the KR of all sub-bands.

To find out the optimal Q, the exhaustive searching method is utilized. The searching ranges is set (1, $Q_{\max}$) and the step is set to 0.2 by experience. Take the bearing vibration signal x for example. The algorithm of improved TQWT based on KR can be illustrated as follows.

Step 1: Get the length N of x and the maximum fault characteristic frequency $f_{\max}$.

Step 2: Initialize the parameters, $r = 3$, $Q = Q_{\text{temp}} = 1$, $\text{KR}_{\max} = 0$.

Step 3: Calculate J according to equation (22) and decompose x into $J+1$ sub-bands.

Step 4: Calculate KR of all sub-bands to find the max one as KR_{temp}.

Step 5: Get the max KR and the corresponding Q, if $\text{KR}_{\text{temp}} > \text{KR}_{\max}$, let $\text{KR}_{\max} = \text{KR}_{\text{temp}}$ and $Q = Q_{\text{temp}}$.

Step 6: Update the Q_{temp}, $Q_{\text{temp}} = Q_{\text{temp}} + 0.2$.

Step 7: Repeat from step 3 to step 7 until $Q_{\text{temp}} = Q_{\max}$.

3. Improved TQWT based compound fault diagnosis of rolling bearings

When bearings work in a fault conditions, there will be fault characteristic frequency correspond to the fault type. The fault characteristic frequency of bearings can be calculated according to table 1.

Where n is the bearing speed, the unit is r/s. BPI is the frequency of ball pass inner race. BPO is the frequency of ball pass outer race. BS is the spin frequency of the ball. FT is the cage train frequency. Both BPI, BPO, BS and FT are usually provided by bearing manufacturers.

Hilbert envelope is a classical method, which has been widely used in fault feature extraction [29]. The fault characteristic frequency can be obtained from Hilbert envelopes of the sub-bands with fault features. So, a compound fault diagnosis method was proposed based on the improved TQWT and Hilbert envelope in this section. The procedure of the method is shown in figure 3. It includes three main steps, which are detailed as follows.

Step 1: Data acquisition. Bearing vibration signals are obtained through the acceleration sensor and signal acquisition card. And a piece of the vibration signal with length N is taken for analyzing.

Step 2: Decomposition of vibration signal by the improved TQWT. The optimal parameters Q and J of the TQWT are selected firstly. Then, the vibration signal is decomposed into several sub-bands by the improved TQWT. Finally, all sub-bands are sorted descending according to the KR.

Step 3: Fault feature extraction and separation via Hilbert envelope. Hilbert envelope analysis is conducted on the sub-bands and the fault characteristic frequencies are obtained from the Hilbert envelope. Compare them to the fault characteristic frequencies calculated by formula and the fault types can be determined and compound fault diagnosis of bearings is achieved.

Because the KR can better optimize the parameters of TQWT, the vibration signals will be effectively decomposed in to a serial of sub-bands. All sub-bands sub-bands contain fault features and each sub-band is a single fault signals. Sub–bands with different fault features will be isolated and ordered descending according to KR.

4. Simulation and experiment analysis

4.1. Simulation analysis

The simulation signal of rolling bearings with inner race fault and outer race fault can be expressed as follows [4, 30–33]:

$$\begin{cases} x_{i+o}(t) = x_i(t) + x_o(t) + x_n(t) \\ x_i(t) = \sum_{j=1}^{M} A_i(t) \bullet g(t - n/f_i - \lambda/f_i) \\ A_i(t) = \rho(mg\cos(2\pi f_r t + \psi_{mi}) + me\omega^2\cos(\psi_{ti})) \\ x_o(t) = \sum_{j=1}^{M} A_o(t) \bullet g(t - n/f_o - \lambda/f_o) \\ A_o(t) = \rho(mg\cos(\psi_{mo}) + me\omega^2\cos(2\pi f_r t + \psi_{to})) \\ g(t) = e^{-Bt}\cos(2\pi f_n t) \end{cases} \tag{23}$$

where $x_{\text{i}}(t)$ and $x_{\text{o}}(t)$ are the simulation signal of rolling bearings with inner race fault and outer race fault, respectively. $x_{\text{n}}(t)$ is the noise obeying gauss distribution. f_{i} and f_{o} are the inner race fault characteristic frequency and outer race fault characteristic frequency. λ/f_{i} and λ/f_{o} are the minor slippage around the average period of $1/f_{\text{i}}$ and $1/f_{\text{o}}$. M is the number

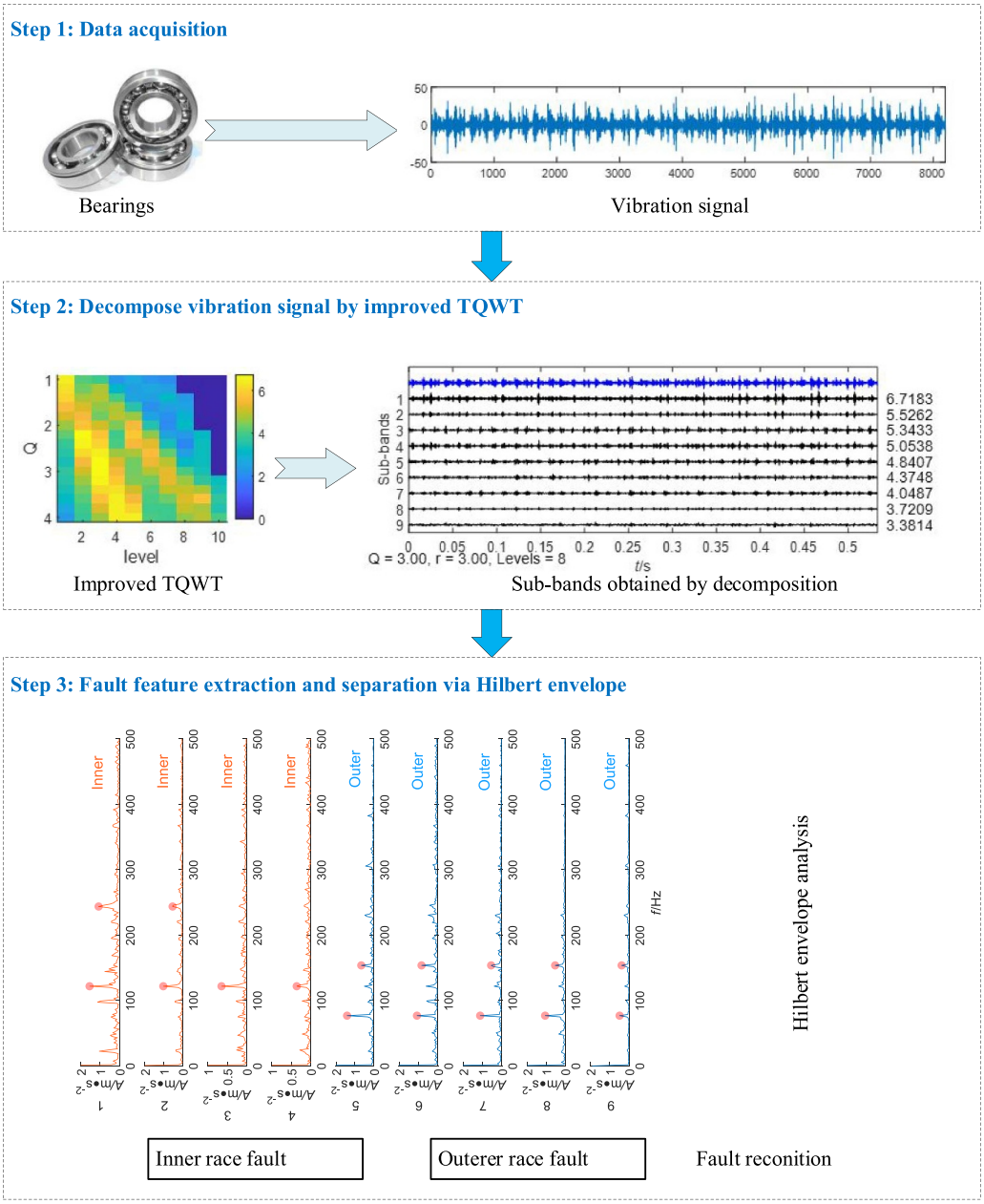

Figure 3. Flow chart of compound fault diagnosis.

of the impulses. $A_i(t)$ and $A_o(t)$ are the amplitude modulator. ρ is the factor between amplitude and load. m, g and e are the rotor mass, gravity acceleration and eccentricity, respectively. f_r is the rotational frequency of bearing. ω is the bearing angular velocity. ψ_{mi} is the angle between gravity direction and inner race defect position. ψ_{ti} is the angle between mass eccentric position and inner race defect position. ψ_{mo} is the angle between gravity direction and outer race defect position. ψ_{to} is the angle between mass eccentric position and outer race defect position. B is the decaying coefficient. f_n is the system natural frequency.

In order to prove the applicability of the method, SKF6312 rolling bearing with inner race fault and outer race fault was selected to generate the simulation signal. Assume $m =$ 50 kg, $g = 9.8$ m s^{-2}, $e = 0.05$ mm, $\rho = 0.001$, $\psi_{mi} = 0$, $\psi_{ti} = 0$, $\psi_{mo} = 0$, $\psi_{to} = 0, f_r = 50$ Hz, $B = 400, f_n = 2000$ Hz, $\lambda = 0.03$. The f_i and f_o can be calculated as $f_i = 246.26$ Hz and $f_o = 153.74$ Hz. The mean and variance of $x_n(t)$ are set to 0 and 5 respectively. The sampling frequency is 10.24 kHz and the number of sample point is 8192. The waveform and spectrum of the simulation signal are shown in figure 4.

The proposed method is applied to analyze the simulation signal to determine the fault type. The first step is to select the parameters of TQWT. In order to reduce computation and ensure decomposition performance, the Q_{max} is set to 4 and the r is set to 3. After 16 iterations, the optimal parameters are obtained as $Q = 1.2$ and $J = 4$. Figure 5 shows theKRs of all sub-bands obtained by TQWT with different Q and J. Only five significant digits are reserved for convenience of presentation. The left axis is Q in the range of 1–4 in 0.2 steps. The

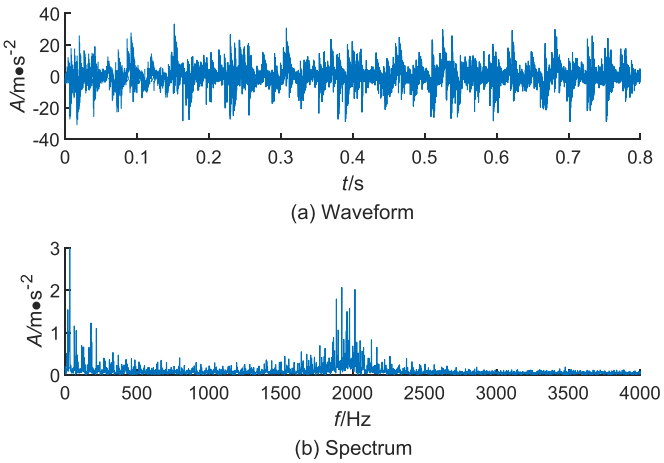

Figure 4. Waveform and spectrum of the simulation signal.

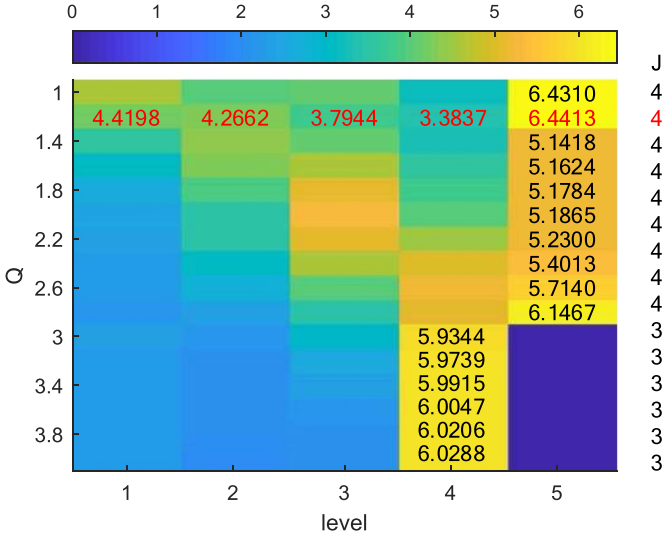

Figure 5. KR of all sub-bands obtained by TQWT with different Q and J.

right axis is J, whose value is 4 or 3. The lower axis is sub-band level. Each rectangle represents a sub-band. The number is the KR of the sub-band. It shows that the biggest KR is obtained as 6.4247 when $Q = 1.2$ and $J = 4$. Then, five sub-bands can be obtained, and the KR of each sub-band from level 1 to level 5 is 4.1002, 4.2283, 3.7654, 3.3490 and 6.4247 respectively, which is marked red. In the process of iteration, Q and J are set to other parameters, and only the biggest KR is shown in the figure, they are little than 6.4247 ($Q = 1.2$ and $J = 4$). So, the optimal parameter combination is $r = 3$, $Q = 1.2$ and $J = 4$. Figure 6 shows the wavelets and frequency response of TQWT with the optimal parameters. It shows the 4 wavelets and its frequency response. We can see that the frequency response covers all the frequency of the simulation signal. It can be well used to decompose the simulation signal.

The simulation signal is decomposed by the improved TQWT and five sub-bands are obtained. Table 2 shows the five sub-bands with different indexes. The first column shows the sub-bands in descending order according to different indexes.

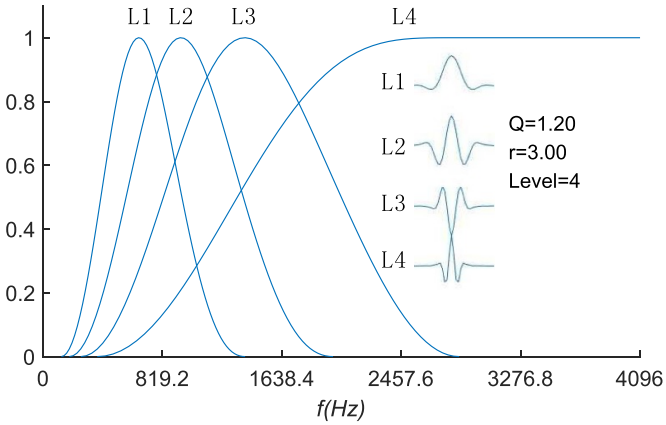

Figure 6. Wavelets and frequency response of TQWT.

Table 2. Five sub-bands with different indexes.

	Decomposition level: indexes		
Sub-bands descend	KR	Kurtosis	RMS
1	5: 6.4413	4: 6.0421	5: 8.2606
2	2: 4.2662	3: 5.9726	1: 3.8738
3	1: 4.1498	2: 4.9991	2: 3.7111
4	3: 3.7944	1: 4.5144	3: 2.1450
5	4: 3.3837	5: 4.0390	4: 1.3706
Weight		0.4309	0.5691

The other columns are the decomposition level with different indexes. We can see that the sub-bands and the decomposition level are disrupted. The last row contains the weight of kurtosis and RMS. They are 0.4309 and 0.5691 respectively. Take the first sub-band for example, the decomposition level 5 has the biggest KR 6.4413 and the RMS 8.2606, but the kurtosis is the 4.0390, which is the smallest kurtosis, The KR can be calculated according to the equation (19).

$$\mathrm{KR} = 0.4309 \times 4.0390 + 0.5691 \times 8.2606 \approx 6.4415. \quad (24)$$

In fact the KR is 6.4413, this error is caused by the reservation of only five significant digits.

The waveform of sub-bands sorted descending according to KR is shown in figure 7. It can be seen that all sub-bands have impact vibration, namely all sub-bands have fault features.

Hilbert envelope analysis is carried out on the five sub-bands as shown in figure 8. We can see that there are frequencies of 152.5 Hz and its multiple frequencies in the first two sub-bands. It is close to the fault characteristic frequencies of outer race 153.74 Hz. So, it can be determined that the bearing had a fault in the outer race. Furthermore, there are frequencies of 243.75 Hz and its multiple frequencies in the last three sub-bands. It is close to the fault characteristic frequencies of inner race 246.26 Hz. It means that the bearing had a fault in the inner race else. So, the conclusion is that the bearing had a compound fault of inner and outer race. It is coincident with the fact. We also can see that the outer race fault features are only in the first two sub-bands and inner race fault features are only in the last three sub-bands, namely the fault features

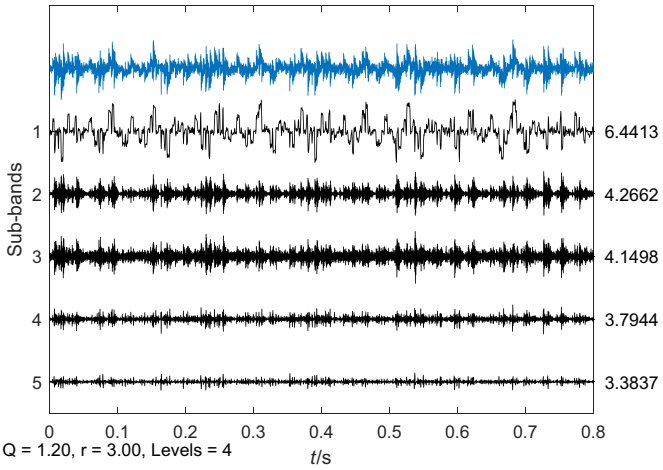

Figure 7. Waveform of all sub-bands obtained by TQWT optimized by KR.

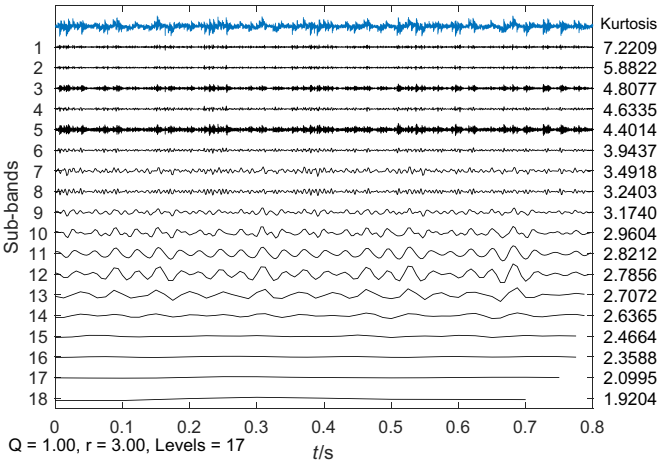

Figure 9. The waveform of all sub-bands sorted descending according to kurtosis.

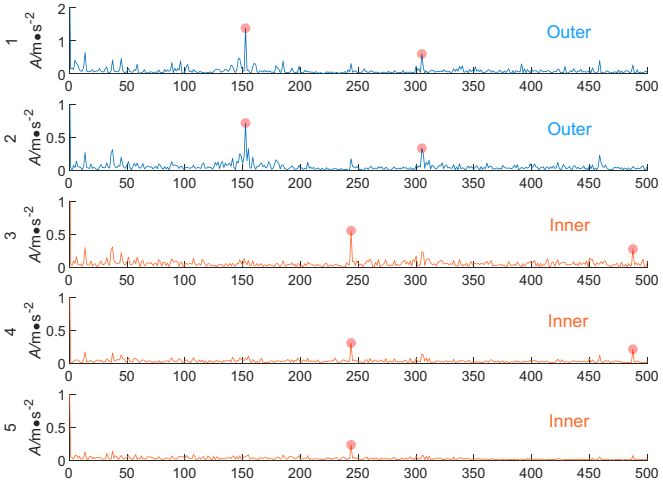

Figure 8. Hilbert envelopes of the five sub-bands.

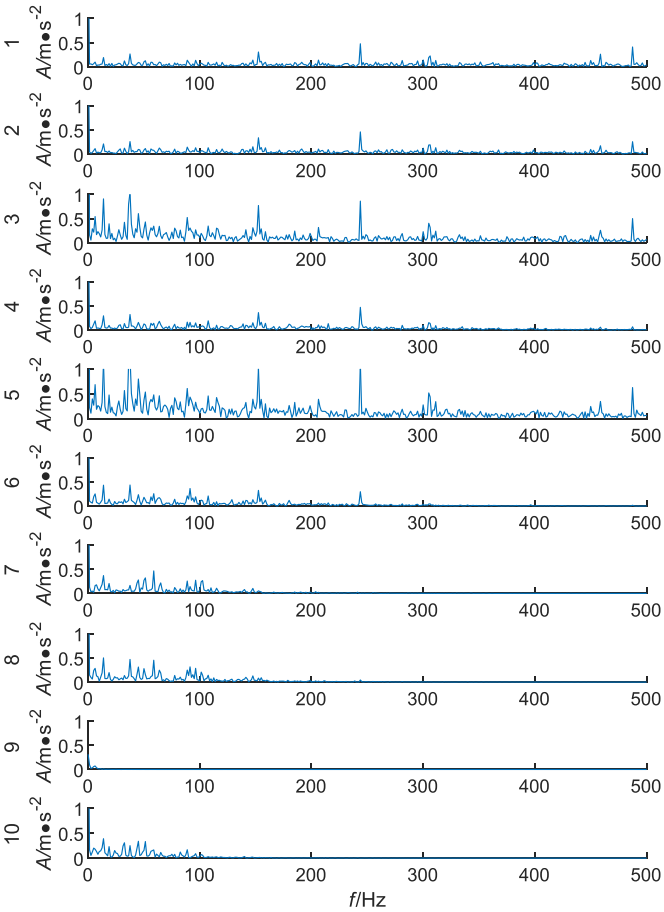

Figure 10. Hilbert envelopes of the first ten sub-bands.

are isolated. That makes compound fault diagnosis of rolling bearings more convenient and accurate.

In order to prove the advantages of the proposed method, diagnosis analysis based on the TQWT optimized by kurtosis is conducted as a comparison. The kurtosis is taken as the performance indexes of the TQWT. The r is set to 3. In order to reduce computation and ensure decomposition performance, the $Q_{\max}$ is set to 4. And the decomposition level is calculated according to equation (14), which is not optimized. After 16 iterations, the parameters are obtained as $Q = 1$ and $J = 17$.

There are 18 sub-bands after the simulation signal decomposed by the TQWT with the parameter $r = 3$, $Q = 1$ and $J = 17$. Figure 9 shows the waveform of all sub-bands sorted descending according to kurtosis. It is obvious that not all sub-bands contain the fault features. It is generally considered that a sub-band contains fault characteristics when its kurtosis greater than 3. So, the first nine sub-bands should by analyzed by Hilbert envelope. In order to better observe the decomposition results, Hilbert envelope analysis is carried out on the first ten sub-bands as shown in figure 10. We can see that the fault characteristic frequencies mainly exist in the first six sub-bands. And the fault characteristic frequencies of inner race and outer race are not separated.

Comparison result shows that the index KR can take advantages of kurtosis and RMS and KR can be better used for improving the TQWT. The improved TQWT can adaptively

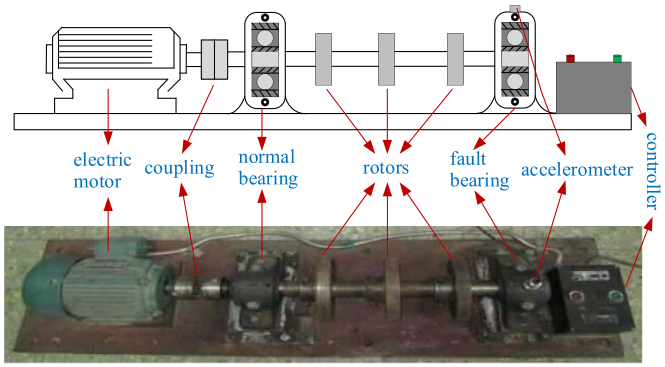

Figure 11. Rotating machinery fault simulation platform.

Figure 12. Faulty bearing.

determine the optimal parameters Q and J of TQWT. The bearing vibrational signal can be well decomposed into a serial of sub-bands by the improved TQWT, the number of sub-bands is small and each sub-band has the fault features. So, the Hilbert envelope analysis can be carried out on all the sub-bands and the compound faults can be separated and determined.

4.2. Experiment analysis

4.2.1. Data source. In order to prove the validity of the proposed method, a compound fault diagnosis experiment was carried out. The experimental data are obtained from the rotating machinery fault simulation platform, as shown in figure 11. It is consisted of an electric motor, a coupling, a normal bearing, three rotors, a controller and a faulty bearing with the type 6307, which is adopted to collect the vibrational signal. The faulty bearing is shown in figure 12, it shows that the bearing has a compound fault of inner race and outer race. The motor speed is 1496 rpm, which means the rotation frequency is 24.93 Hz. The fault characteristic frequency of outer race is 76.31 Hz, and the fault characteristic frequency of inner race is 123.13 Hz. The accelerometer is mounted vertically on the bearing seat. The sampling frequency is 15.36 kHz and the number of sample point is 8192.

The waveform and spectrum of the vibration signals of normal bearing and fault bearing with a compound fault of inner race and outer race are shown in figure 13. It shows that the

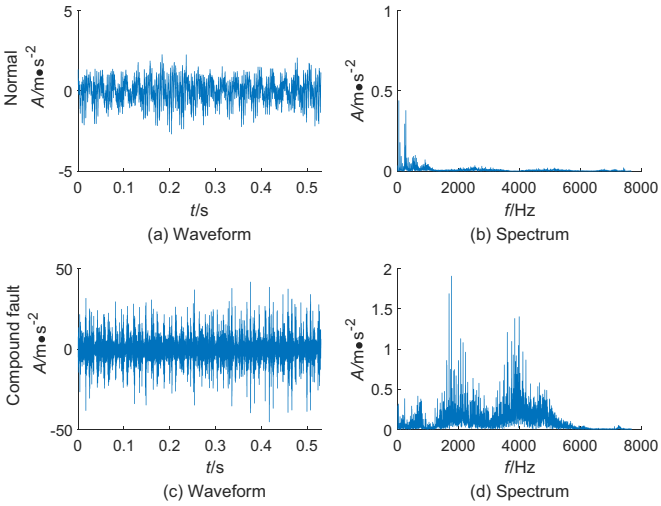

Figure 13. Waveform and spectrum of the vibration signal of normal bearing and fault bearing.

amplitude increases sharply and high frequency impact vibration occurs when the bearing works in compound fault condition. We can see the bearing is damaged from the waveform and spectrum, but cannot determine the fault type.

4.2.2. Proposed method. In order to determine the fault type, the proposed method is used to analyze the vibration signal of the bearing with a compound fault of inner race and outer race. The first step is the selection of the parameters of TQWT. The r is set to 3. In order to reduce computation and ensure decomposition performance, the $Q_{\max}$ is set to 4. After 16 iterations, the optimal parameters are obtained as $Q = 3$ and $J = 8$. Figure 14 shows the *KR*s of all sub-bands obtained by TQWT with different Q and J. Only five significant digits are reserved for convenience of presentation. The left axis is Q in the range of 1–4 in 0.2 steps. The right axis is J, whose value is 6, 7, 8 or 9. The lower axis is sub-band level. Each rectangle represents a sub-band. The number is the KR of the sub-band. It shows that the biggest KR is obtained as 6.7183 when $Q = 3$ and $J = 8$. Then, nine sub-bands can be obtained, and the KR of all sub-band from level 1 to level 9 are 3.7209, 5.0538, 6.7183, 5.5262, 4.3748, 4.8407, 5.3433, 4.0487 and 3.3814 respectively, which are marked red. In the process of iteration, Q and J are set to other parameters, and only the biggest KR is shown in the figure, they are little than 6.7183 ($Q = 3$ and $J = 8$). So, the optimal parameter combination is $r = 3$, $Q = 3$ and $J = 8$.

Figure 15 shows the wavelets and frequency response of TQWT with the optimal parameter. It shows the eight wavelets and its frequency response. We can see that the frequency response covers the main frequency of the vibrational signal. It can be well used to decompose the vibrational signal.

The vibration signal is decomposed by the improved TQWT and nine sub-bands are obtained. Table 3 shows the nine sub-bands with different indexes. The first column is the sub-bands in descending order according to different indexes. The other columns are the decomposition levels with different

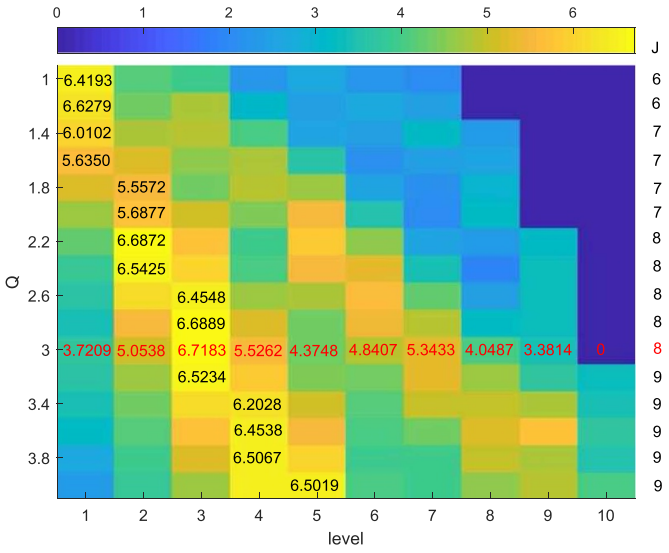

Figure 14. KR of all sub-bands obtained by TQWT with different Q and J.

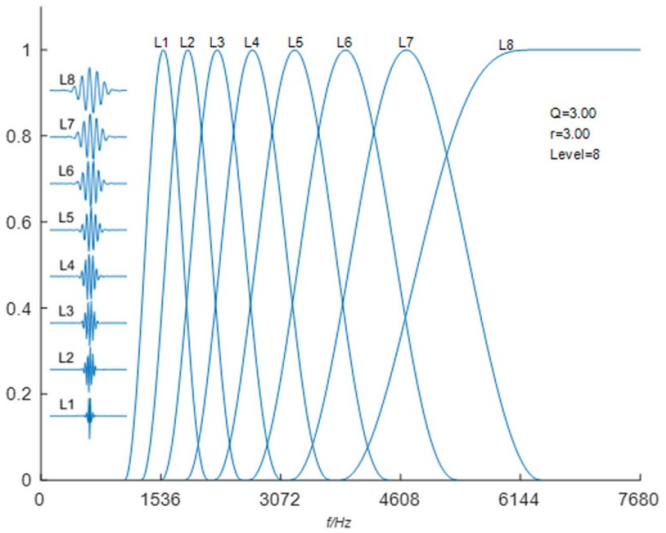

Figure 15. Wavelets and frequency response of TQWT optimized by KR.

indexes. We can see that the sub-bands and the decomposition level are disrupted. The last row contains the weight of kurtosis and RMS. They are 0.4094 and 0.5906 respectively. Take the first sub-band for example, the decomposition level 3 has the biggest KR 6.7183 and the RMS 5.9065, but the kurtosis is 7.8892, which is not the biggest kurtosis, The KR can be calculated according to the equation (19):

$$\mathrm{KR} = 0.4094 \times 7.8892 + 0.5906 \times 5.9065 \approx 6.7182. \quad (25)$$

In fact the KR is 6.7183, this error is caused by the reservation of only five significant digits.

The waveform of sub-bands sorted descending according to KR is shown in figure 16. From figure 16 we can see that all sub-bands have impact vibration, namely all sub-bands have fault features.

Table 3. Nine sub-bands with different indexes.

	Decomposition level: indexes		
Sub-bands descend	KR	Kurtosis	RMS
1	3: 6.7183	4: 8.5437	3: 5.9065
2	4: 5.5262	3: 7.8892	7: 5.2932
3	7: 5.3433	1: 6.1465	6: 4.6871
4	2: 5.0538	2: 5.8046	2: 4.5333
5	6: 4.8407	5: 5.6626	8: 4.0213
6	5: 4.3748	7: 5.4154	5: 3.4819
7	8: 4.0487	6: 5.0622	4: 3.4341
8	1: 3.7209	8: 4.0883	9: 3.0170
9	9: 3.3814	9: 3.9069	1: 2.0391
Weight		0.4094	0.5906

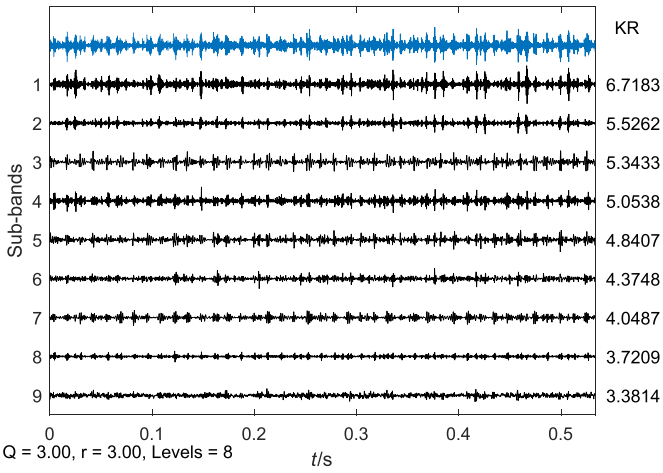

Figure 16. Waveform of all sub-bands obtained by TQWT optimized by KR.

Hilbert envelope analysis is carried out on the nine sub-bands as shown in figure 17. It can be seen that there are frequencies of 121.875 Hz in the first four sub-bands. It is close to the fault characteristic frequencies of inner race 123.13 Hz. The doubling frequencies are also found. So, it can be determined that the bearing had a fault in the inner race. Furthermore, there are frequencies of 76.875 Hz and its multiple frequencies in the last five sub-bands. It is close to the fault characteristic frequencies of outer race 76.31 Hz. Which means that the bearing had a fault in the outer race else. So, the conclusion is that the bearing had a compound fault of inner and outer race. It is coincident with the fact. We also can see that the inner race fault features are only in the first four sub-bands and outer race fault features are only in the last five sub-bands, namely the fault features are isolated. That makes compound fault diagnosis of rolling bearings more convenient and accurate.

4.2.3. Compared method. In order to further demonstrate the effectiveness of this method, the kurtosis and RMS are used to optimize the parameters of TQWT as comparisons.

TQWT optimized by kurtosis was took as the first comparison. The r is set to 3 and the $Q_{\max}$ is set to 4, which is the same as proposed method. The kurtosis of all sub-bands

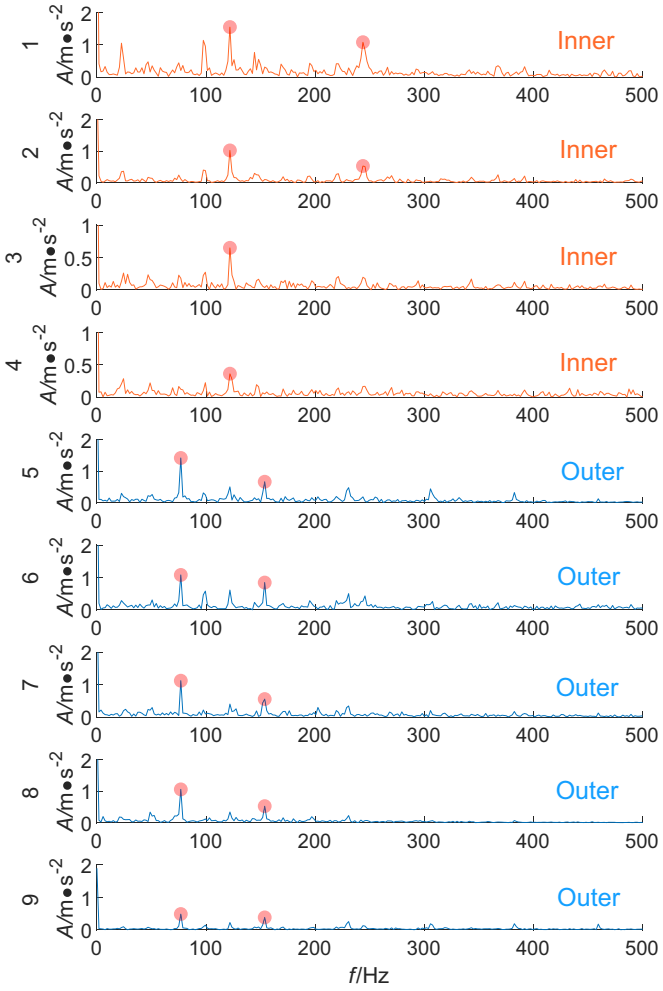

Figure 17. Hilbert envelopes of the nine sub-bands.

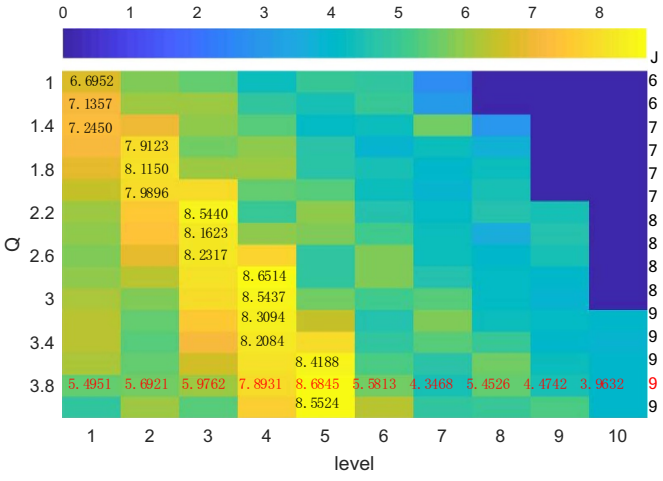

Figure 18. Kurtosis of all sub-bands obtained by TQWT with different Q and J.

obtained by TQWT with different Q and J are shown in figure 18. Only five significant digits are reserved for convenience of presentation. The left axis is Q in the range of 1–4 in 0.2 steps. The right axis is J, whose value is 6, 7, 8 or 9. The

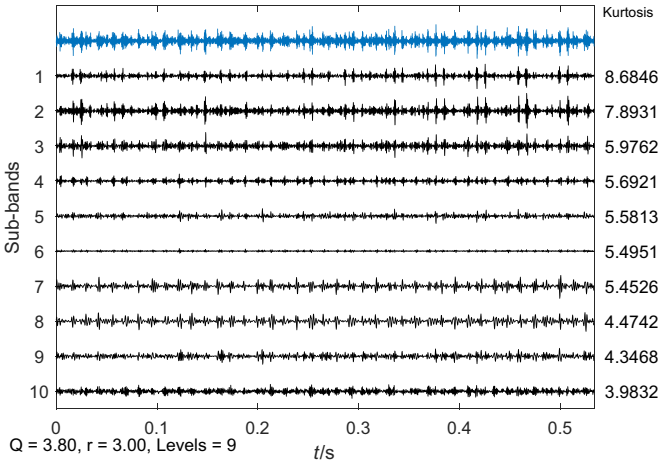

Figure 19. Waveform of sub-bands sorted descending according to kurtosis.

lower axis is sub-band level. Each rectangle represents a sub-band. The number is the kurtosis of the sub-band. It shows that the biggest kurtosis is obtained as 8.6845 when $Q = 3.8$ and $J = 9$. Then, ten sub-bands are obtained, and the kurtosis of all sub-band from level 1 to level 10 are 5.4951, 5.6921, 5.9762, 7.8931, 8.6845, 5.5813, 4.3468, 5.4526, 4.4742 and 3.9632 respectively, which are marked red. In the process of iteration, Q and J are set to other parameters, and only the biggest KR is shown in the figure, they are little than 8.6845 ($Q = 3.8$ and $J = 9$). So, the optimal parameter combination is $r = 3$, $Q = 3.8$ and $J = 9$.

The vibration signal is decomposed into ten sub-bands by TQWT with the parameters. The waveform of sub-bands sorted descending according to kurtosis are shown in the figure 19. It shows that the 6th sub-band does not have obvious features. The Hilbert envelopes analysis of the ten sub-bands are shown in figure 20. We can see that there are frequencies of 121.875 Hz and the doubling frequencies in the first two sub-bands. It is close to the fault characteristic frequencies of outer race 123.13 Hz. And there are frequencies of 76.875 Hz and its multiple frequencies in the 4th, 7th, and 8th sub-bands. It is close to the fault characteristic frequencies of inner race 76.31 Hz. But for the 3rd and 9th sub-bands there are both frequencies of 121.875 Hz and 76.875 Hz. Which means that the fault features are not separated. For the 5th sub-band, there is only frequencies of 121.875 Hz, in addition, there are not obvious features in the 6th sub-band. It is obvious that the features of sub-bands obtained by the TQWT optimized by kurtosis are not separated. So, the proposed improved TQWT has a better decomposition performance.

Next, let us take TQWT optimized by RMS as the second comparison. The parameters of r and $Q_{\max}$ is same as the proposed method. The RMS of all sub-bands obtained by TQWT with different Q and J are shown in figure 21. After 16 iterations, the optimal parameters $Q = 3.6$ and $J = 9$ are obtained. The vibration signal is decomposed into ten sub-bands by TQWT with the parameters. The waveform of sub-bands sorted descending according to RMS are shown in the figure 22. It is obvious that the 10th sub-band does not

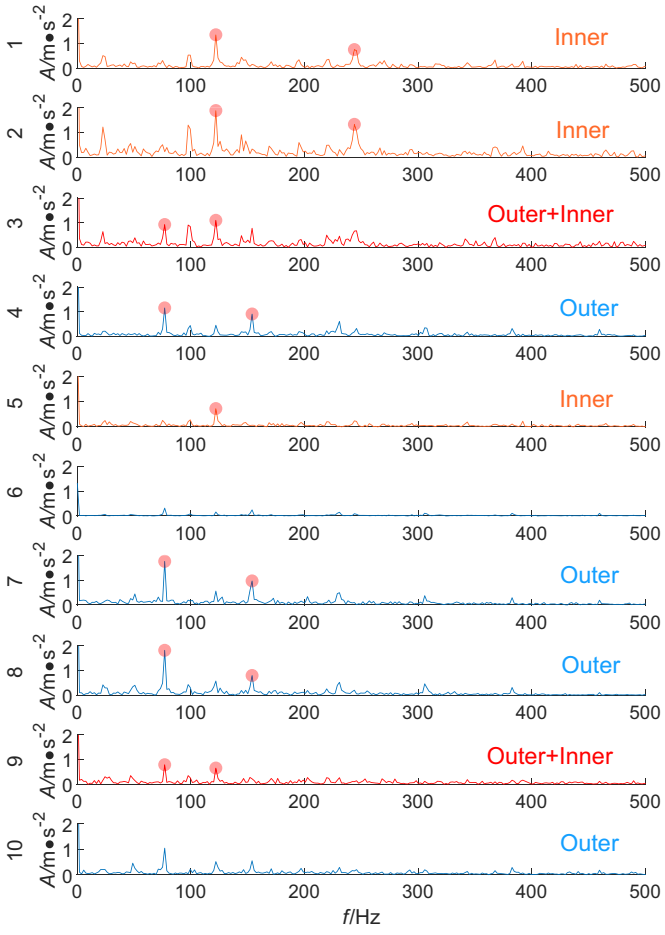

Figure 20. Hilbert envelopes of the ten sub-bands.

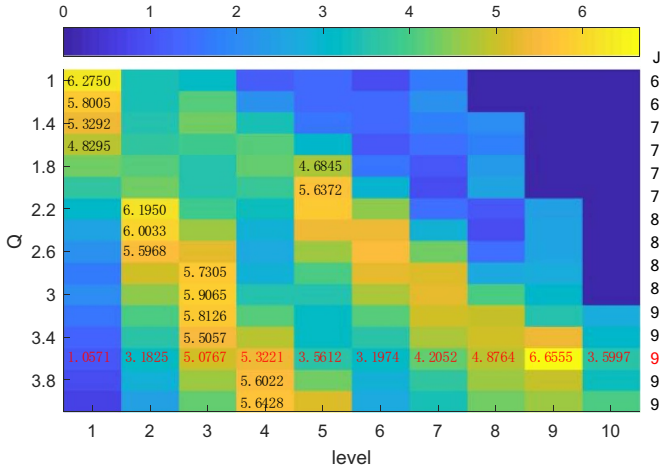

Figure 21. RMS of all sub-bands obtained by TQWT with different Q and J.

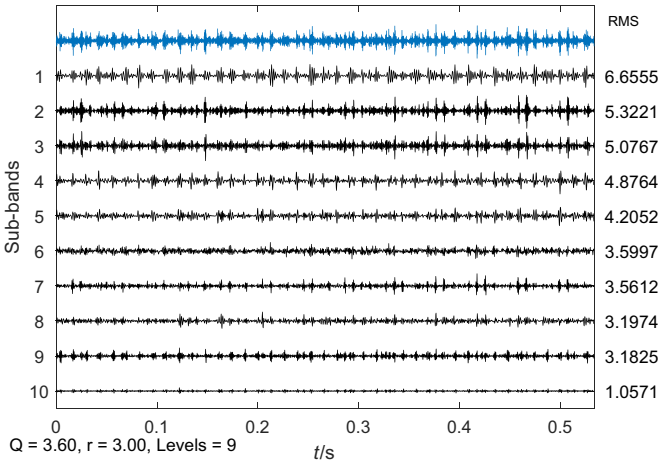

Figure 22. Waveform of sub-bands sorted descending according to RMS.

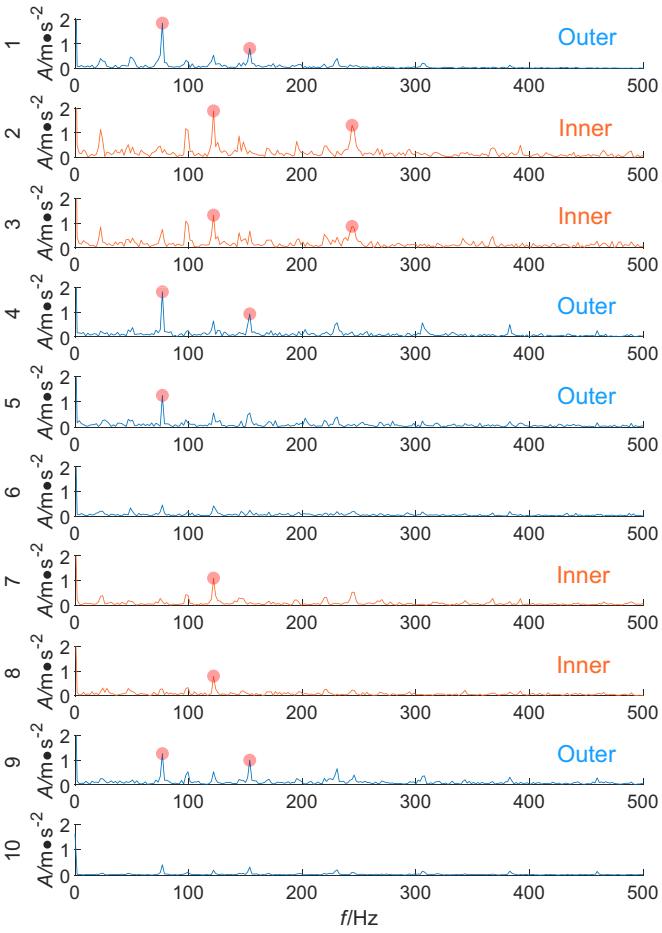

Figure 23. Hilbert envelopes of the ten sub-bands.

has obvious fault features. The Hilbert envelopes of the ten sub-bands are shown in figure 23. We can see that there are frequencies of 76.31 Hz and the doubling frequencies in the 1st, 4th and 9th sub-bands. It is close to the fault characteristic frequencies of outer race 76.875 Hz. There are frequencies of 121.875 Hz and its multiple frequencies in the 2nd and 3rd sub-bands. It is close to the fault characteristic frequencies of outer race 123.13 Hz. But for the 5th, 7th and 8th sub-bands there are not the multiple frequencies. And the 6th and 10th sub-bands does not have obvious features. Even though, the features are separated, but they are not sorted by the rms.

5. Conclusions

In this paper, a novel method of compound fault diagnosis of rolling bearings based on improved TQWT is proposed. In this method, the TQWT is improved by a new evaluation index KR, the Q-factor and decomposition level can be determined at the same time. The performance of the proposed method is verified by the analysis of both simulation and experiment. The result shows that KR takes advantages of kurtosis and RMS, making it better to be used for improving the TQWT. In the improved TQWT, the key parameters Q-factor and decomposition level can be simultaneously and adaptively determined according to the vibration signal. The vibration signal can be effectively decomposed into a serial of sub-bands by the improved TQWT. All sub-bands contain fault features and the different fault features are separated into the different sub-bands, the fault type can be easily and accurately identified. In the future research, the improved kurtosis will be used for the optimization of other decomposition method such as empirical mode decomposition, local mean decomposition, variational mode decomposition, *et al*. And the improved TQWT will be used for feature extraction with other feature extraction method such as entropy to improve the accuracy of fault classification model such as support vector machine, extreme learning machine, neural networks, *et al*. In real application, the operating conditions of bearings such as load and speed are constantly changing and the fault diagnosis of bearings under variable conditions is still not be solved. So, the future work will focus on the compound fault diagnosis of bearings under variable conditions.

Data availability statement

No new data were created or analysed in this study.

Acknowledgments

This work was supported in part by the Science and Technology Research Project of Henan Province under Grant No. 202102210061, the Key Scientific Research Projects of Universities in Henan under Grant Nos. 19B460001, 20B470002, 21B470003, and the Doctoral Research Fund of Henan Institute of Technology under Grant No. KQ1807. The authors also thank the anonymous reviewers and referees for their valuable comments and suggestions.

ORCID iDs

Yongtao Hu https://orcid.org/0000-0003-1800-3683
Yonggang Xu https://orcid.org/0000-0002-2206-8968

References

[1] Leite G N P, Araújo A M, Rosas P A C, Stosic T and Stosic B 2019 Entropy measures for early detection of bearing faults *Physica* A **514** 458–72
[2] Lei Y G, Yang B, Jiang X W, Jia F, Li N P and Nandi A K 2020 Applications of machine learning to machine fault diagnosis: a review and roadmap *Mech. Syst. Signal Process.* **138** 106587
[3] Tang G and Tian T 2020 Compound fault diagnosis of rolling bearing based on singular negentropy difference spectrum and integrated fast spectral correlation *Entropy* **22** 367
[4] Zhang K, Xu Y, Liao Z, Song L and Chen P 2021 A novel Fast Entrogram and its applications in rolling bearing fault diagnosis *Mech. Syst. Signal Process.* **154** 107582
[5] Wu P, Nie X and Xie G 2021 Multi-sensor signal fusion for a compound fault diagnosis method with strong generalization and noise-tolerant performance *Meas. Sci. Technol.* **32** 035108
[6] Wan S T and Peng B 2019 The FERgram: a rolling bearing compound fault diagnosis based on maximal overlap discrete wavelet packet transform and fault energy ratio *J. Mech. Sci. Technol.* **33** 157–72
[7] Qin C R, Wang D D, Xu Z and Tang G 2020 Improved empirical wavelet transform for compound weak bearing fault diagnosis with acoustic signals *Appl. Sci.* **10** 682
[8] Pan H Y, Yang Y, Li X, Zheng J D and Cheng J S 2019 Symplectic geometry mode decomposition and its application to rotating machinery compound fault diagnosis *Mech. Syst. Signal Process.* **114** 189–211
[9] Purushotham V, Narayanan S and Prasad S A N 2008 Multi-fault diagnosis of rolling bearing elements using wavelet analysis and hidden Markov model based fault recognition *NDT & E Int.* **38** 654–64
[10] Dhamande L S and Chaudhari M B 2018 Compound gear-bearing fault feature extraction using statistical features based on time-frequency method *Measurement* **125** 63–77
[11] Chen J, Zi Y, He Z and Yuan J 2013 Compound faults detection of rotating machinery using improved adaptive redundant lifting multiwavelet *Mech. Syst. Signal Process.* **38** 36–54
[12] Tang B P, Liu W Y and Song T 2010 Wind turbine fault diagnosis based on Morlet wavelet transformation and Wigner-Ville distribution *Renew. Energy* **35** 2862–6
[13] Selesnick I W 2011 Wavelet transform with tunable Q-factor *IEEE Trans. Signal Process.* **59** 3560–75
[14] Wang H Q, Ke Y L, Luo G G and Tang G 2016 Compressive sensing of roller bearing fault using tunable Q-factor wavelet transform *IEEE Int. Instrumentation and Measurement Technology Conf. Proc.* (*Taipei, Taiwan, China, 23 May 2016*) (https://doi.org/10.1109/I2MTC.2016.7520336)
[15] Xiang W W, Cai G G, Fan W, Huang W G and Zhu Z K 2015 Transient feature extraction based on double-TQWT and its application in bearing fault diagnosis *J. Vib. Shock* **34** 34–9
[16] Upadhyay N and Kankar P K 2018 Diagnosis of bearing defects using tunable Q-wavelet transform *J. Mech. Sci. Technol.* **32** 549–58
[17] Zhao J L, Zhang Y C and Chen Q G 2020 Rolling bearing fault feature extraction based on adaptive tunable Q-factor wavelet transform and spectral kurtosis *Shock Vib.* **2020** 8875179
[18] Li H, Liu T, Wu X and Chen Q 2019 Application of optimized variational mode decomposition based on kurtosis and resonance frequency in bearing fault feature extraction *Trans. Inst. Meas. Control* **42** 518–27
[19] Dibaj A, Hassannejad R, Ettefagh M M and Ehghaghi M B 2021 Incipient fault diagnosis of bearings based on parameter-optimized VMD and envelope spectrum weighted kurtosis index with a new sensitivity assessment threshold *ISA Trans.* **114** 413–33
[20] Qin Y, Xing J and Mao Y 2016 Weak transient fault featureextraction based on an optimized Morlet wavelet and kurtosis *Meas. Sci. Technol.* **27** 085003

[21] Xu Y G, Fan Z Y, Zhang K and Ma C Y 2019 A novel method for extracting maximum kurtosis component and its applications in rolling bearing fault diagnosis *Shock Vib.* **2019** 8218237
[22] Li Q and Liang S Y 2018 Bearing incipient fault diagnosis based upon maximal spectral kurtosis TQWT and group sparsity total variation denoising approach *J. Vibroeng.* **20** 1409–25
[23] Wang X L, Tang G J and Zhou F C 2017 Application of adaptive tunable Q-factor wavelet transform on incipient fault diagnosis of bearing *J. Aerosp. Power* **32** 2647–475
[24] Ma P, Zhang H L, Fan W H and Wang C 2019 Early fault diagnosis of bearing based on frequency band extraction and improved tunable Q-factor wavelet transform *Measurement* **137** 189–202
[25] Piltan F and Kim J-M 2021 Fault diagnosis of bearings using an intelligence-based autoregressive learning Lyapunov algorithm *Int. J. Comput. Intell. Syst.* **14** 537–49
[26] Daubechies I 1992 Time-frequency density and orthonormal bases *Ten lectures on wavelets* (Philadelphia, Pennsylvania, USA: Siam) pp 107–28
[27] Li Y B, Liang X H, Xu M Q and Huang W H 2016 Early fault feature extraction of rolling bearing based on ICD and tunable Q-factor wavelet transform *Mech. Syst. Signal Process.* **86** 204–23
[28] He W P, Zi Y Y, Chen B Q, Wu F and He Z J 2015 Automatic fault feature extraction of mechanical anomaly on induction motor bearing using ensemble super–wavelet transform *Mech. Syst. Signal Process.* **54–55** 457–80
[29] Song H J, Lei W P, Niu Z Y and Meng Y J 2019 Instantaneous amplitude-frequency feature extraction for rotor fault based on BEMD and Hilbert transform *Shock Vib.* **2019** 1639139
[30] Zhang M, Jiang Z N and Feng K 2017 Research on variational mode decomposition in rolling bearings fault diagnosis of the multistage centrifugal pump *Mech. Syst. Signal Process.* **93** 460–93
[31] Antoni J and Randall R B 2002 Differential diagnosis of gear and bearing faults *J. Vib. Acoust.* **124** 165–71
[32] Antoni J and Randall R B 2003 A stochastic model for simulation and diagnostics of rolling element bearings with localized faults *J. Vib. Acoust.* **125** 282–9
[33] Wu K, Chu N, Wu D and Antoni J 2021 The Enkurgram: a characteristic frequency extraction method for fluid machinery based on multi-band demodulation strategy *Mech. Syst. Signal Process.* **155** 107564